GDCh Research Article Angewandte International Edition Chemie www.angewandte.org

How to cite: Angew. Chem. Int. Ed. 2025, e202500336
doi.org/10.1002/anie.202500336

VIP Porous Materials Very Important Paper

Tunable Catalytic Vertex Wall Chemistry in Metal-free Covalent Organic Frameworks for Enhanced Oxygen Reduction

Changqing Li, Zhaoying Wang, Yucheng Jin, Zhongping Li, Jong-Pil Jeon, Songlin Zhao, Yanhua Shao, Feng Tang, Won-Yeong Kim, Runnan Guan, Jeong-Min Seo, Zonghoon Lee,* Sang-Young Lee,* and Jong-Beom Baek**

Abstract: Metal-free covalent organic frameworks (COFs) have emerged as promising catalysts for the oxygen reduction reaction (ORR) because of their unique structural properties and notable stability. To enhance both catalytic activity and selectivity, a variety of linkers and linkages have been investigated in efforts to precisely engineer COFs. However, the impact of vertex structures within COFs on ORR catalysis remains largely underexplored. Here, to modulate COF catalytic performance, we introduce tunable catalytic vertex wall chemistry by introducing diverse triazine and thiophene units. The catalytic vertex wall approach allows the fine-tuning of electronic surface states, leading to improved intermediate adsorption characteristics and accelerated ORR activity. Remarkably, the engineered COF achieved a half-wave potential of 0.76 V, surpassing COFs modified by linker or linkage strategies. Theoretical calculations suggest that this enhanced activity arises from the strong binding affinity of OOH* intermediates to carbon atoms adjacent to the thiophene vertex, facilitating OOH* reduction to a O_2 molecule, which is the rate-limiting step of the ORR. These findings reveal the pivotal role of vertex wall engineering in conjugated COF frameworks, and offer critical insights to advance COFs design toward superior ORR performance.

Introduction

The oxygen reduction reaction (ORR) is key to clean energy technologies like metal-air batteries and fuel cells.[1] Metal-free carbon-based electrocatalysts are a cost-effective alternative to platinum, with promising potential ORR activity. However, primitive carbon materials often lack effective interaction sites, which limits their ability to adsorb oxygen or activate ORR intermediates.[2] Improving their performance requires modifying the electronic environment or spin distribution of the sp^2 carbon skeletons.[3] Strategies such as defect engineering, heteroatom doping, and high-temperature pyrolysis have already been used to overcome their drawbacks.[1–3] However, achieving precise regulation of the structure, active sites, and defects remains a significant challenge, highlighting the necessity for ongoing research into the development of advanced carbon-based electrocatalysts.

Covalent organic frameworks (COFs) have emerged as a novel class of crystalline materials with predictable and well-defined structures.[4–6] The frameworks are constructed by linking individual organic building blocks through strong covalent bonds, resulting in materials with high surface areas, long-range order, and exceptional stability.[4–7] The versatility of the functional building blocks and topologies makes COFs suitable for a wide range of applications, including optoelectronic materials, energy storage, gas separation, and catalysis.[8–17] With respect to electrocatalytic oxygen reduction reactions, COFs have demonstrated potential advantages for cathode discharge processes in oxygen (hydrogen) evolution reactions.[11,12]

The catalytic activity of COFs for ORR is greatly influenced by their molecular structure, which affects the electronic environment of the active sites.[13] By modifying the organic structural blocks or bonds within the COFs, their conductivity and interactions with O_2 and intermediates can be tuned. Since 2020, various studies have explored different linker and linkage strategies to enhance the catalytic performance of COFs.[13–17] For instance, Yao et al. demonstrated that COFs with thiophene linkers and a high density of heteroatoms exhibited exceptional ORR activity.[13a,b]

[*] Dr. C. Li, Y. Jin, Prof. Z. Li, Dr. J.-P. Jeon, S. Zhao, Dr. Y. Shao, Dr. F. Tang, Dr. R. Guan, Dr. J.-M. Seo, Dr. J.-B. Baek
Department of Energy and Chemical Engineering/Center for Dimension-Controllable Organic Frameworks, Ulsan National Institute of Science and Technology, 50 UNIST-gil, Eonyang-eup, Ulju-gun, Ulsan, 44919, Republic of Korea
E-mail: lizhongping2023@unist.ac.kr
jbbaek@unist.ac.kr

Z. Wang, Prof. Z. Lee
Engineering Center for Multidimensional Carbon Materials, Institute for Basic Science (IBS), 50 UNIST-gil, Eonyang-eup, Ulju-gun, Ulsan, 44919, Republic of Korea

Z. Wang, Prof. Z. Lee
Department of Materials Science and Engineering, Ulsan National Institute of Science and Technology, 50 UNIST-gil, Eonyang-eup, Ulju-gun, Ulsan, 44919, Republic of Korea
E-mail: zhlee@unist.ac.kr

W.-Y. Kim, Prof. S.-Y. Lee
Department of Chemical and Biomolecular Engineering, Yonsei University, 50 Yonsei-ro, Seodaemun-gu, Seoul, 03722, Republic of Korea.
E-mail: syleek@yonsei.ac.kr

Yang and his team employed unsaturated bonds as linkers to modulate the catalytic activity of imine-linked COFs,[13c] while Zeng et al. designed COFs with various linkages, including oxazole, azine, amide, and imine, to optimize ORR performance.[14] Despite these advancements, the crucial role of COF vertex walls in ORR catalysis remains underexplored.

Vertex walls often play a pivotal role by supporting the high-order π skeleton, enhancing self-assembly capability, chemical stability, and electron/charge transfer. Identifying the most suitable vertex configurations for ORR remains an open question.

In this study, we introduce tunable catalytic vertex wall chemistry to modulate the catalytic behaviors of COFs. Catalytic vertex engineering has recently emerged as a groundbreaking strategy to modulate catalytic behaviors by incorporating diverse triazine and thiophene units. This approach leverages the principle that modifying the vertex structures of COFs can profoundly influence their electronic environments and catalytic properties. By employing a catalytic vertex-wall configuration, the electronic states can be finely tuned through variations in conjugation. This precise regulation of electronic states enhances intermediate adsorption capabilities, thereby optimizing ORR activity. Notably, this approach achieves a remarkable half-wave potential of 0.76 V and a mass activity of 14.5 $A g^{-1}$. These values surpass those observed for other linker or linkage-based COFs. The enhanced catalytic performance can be attributed to the stronger binding affinity of *OOH intermediates to the carbon atoms adjacent to the thiophene units, as verified by theoretical calculations. These findings are consistent with transition state theory and recent computational studies that have highlighted the importance of vertex modifications for enhancing catalytic efficiency. The results of this study underscore the critical role of vertex wall chemistry in optimizing COFs for catalytic applications and provides valuable insights for the design of advanced materials with superior performance.

Results and Discussion

Different vertex structures of TT-COFs, incorporating triazine and thiophene units, were meticulously designed and synthesized using solvothermal methods, as illustrated in Figure 1a–c. The vinyl-linkage TT-COF-1 was synthesized from 2,2′,2″-((1,3,5-triazine-2,4,6-triyl)tris([1,1′-biphenyl]-4′,4-diyl))triacetonitrile (TTBTA) and benzo[1,2-b:3,4-b′:5,6-b″]trithiophene-2,5,8-tricarbaldehyde (BTTA) in a mixture of 1,2-dichlorobenzene and n-butanol at 120 °C for 3 days. In contrast, the imine-linkage COFs were synthesized using 4′,4‴,4⁗-(1,3,5-triazine-2,4,6-triyl)tris(([1,1′-biphenyl]-4-amine)) (TTTA) and either 1,4-diaminobenzene, benzo[1,2-b:3,4-b′:5,6-b″]trithiophene-2,5,8-tricarbaldehyde (BTTA), or 5,5′,5″-(benzene-1,3,5-triyl)tris(thiophene-2-carbaldehyde) (BTTTA), in a mixture of 1,2-dichlorobenzene and n-butanol at 120 °C for 3 days. The pre-designed vertex walls yield distinct electronic skeletons, which were further characterized by various analyses.

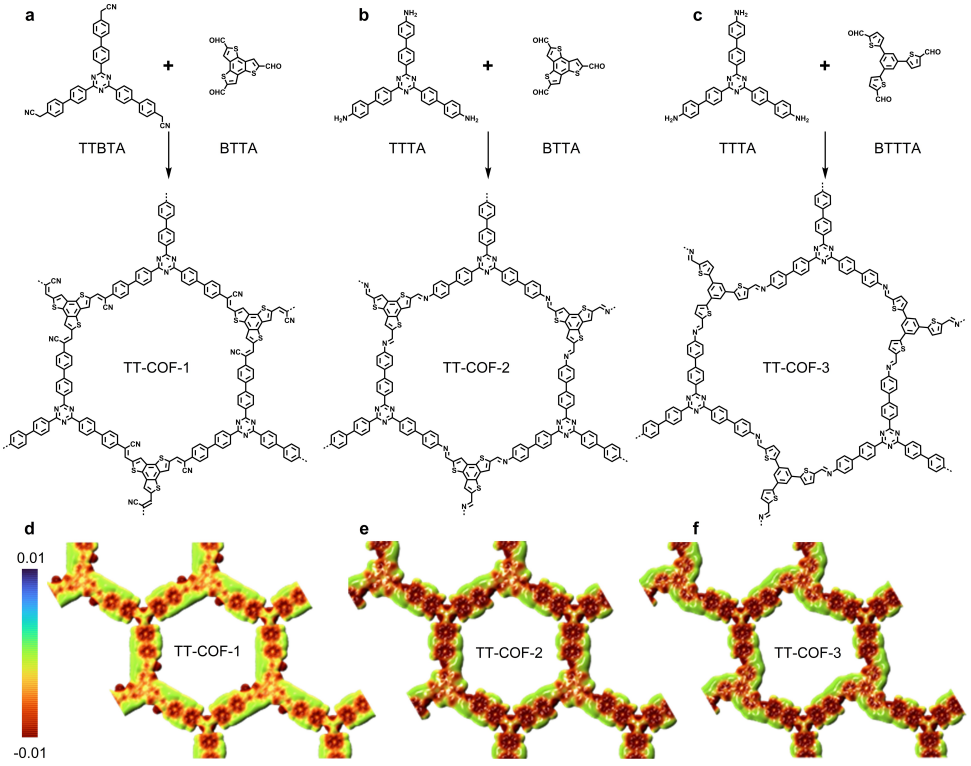

Figure 1. Design and synthesis of (a–c) TT-COFs via tunable vertex wall chemistry. Electrostatic potential mapped surface of (d–f) TT-COFs.

The chemical structures of the TT-COFs were validated through Fourier-transform infrared (FT-IR) spectroscopy (Figure S1). In TT-COF-1, characteristic cyano groups associated with vinyl linkages were observed at 2449 cm^{-1}, while the imine linkages in TT-COF-2 and TT-COF-3 displayed distinct carbon-nitrogen double bond signals at 1627 cm^{-1} and 1628 cm^{-1}, respectively. These spectral signatures confirm the successful formation of the targeted chemical linkages. Additional structural insights were obtained using carbon magic angle spinning solid-state nuclear magnetic resonance (NMR) spectroscopy. For TT-COF-1, characteristic carbon peaks corresponding to vinyl and cyano groups were detected at 108.3 and 117.5 ppm, respectively (Figure S2a). In contrast, the carbon signals of the imine linkages appeared at 149.9 ppm for TT-COF-2 (Figure S2b) and 148.1 ppm for TT-COF-3 (Figure S2c). Additionally, signals detected between 120 and 148 ppm were attributed to aromatic carbon atoms of TT-COFs.

The electrostatic potential surface (ESP) maps of the TT-COFs (Figure 1d–f) provide critical insights into their regulated charge distribution. A gradual extension of negative charges from the triazine vertices to the thiophene vertices was observed, with the effect intensifying from TT-COF-1 to TT-COF-3, consistent with the increasing electronegativity of the thiophene rings. This vertex regulation effectively minimizes uneven charge distribution and optimizes the electronic environment at active sites.

Field-emission scanning electron microscopy (FE-SEM) images further revealed distinct morphologies, with the TT-COFs displaying uniform rod-shaped structures of varying sizes (Figure S3). These morphological differences reflect variations in self-assembly and structural organization, as influenced by the vertex structures. Additionally, energy-dispersive X-ray (EDX) mapping confirmed the uniform distribution of carbon, nitrogen, and sulfur elements across all TT-COFs (Figures S4–S6), verifying the consistent composition of the synthesized materials. The elemental compositions of TT-COFs, including carbon, nitrogen, hydrogen, and sulfur, were experimentally determined and found to be in close agreement with the theoretical values (Table S1).

Porosity and crystallinity, which are crucial characteristics of the three TT-COFs, were assessed using nitrogen sorption at 77 K and powder X-ray diffraction (PXRD) analyses. Nitrogen sorption isotherms revealed that all three COFs exhibited typical type IV isotherms, which are indicative of mesoporous structures, as shown in Figures S7–S9. The Brunauer–Emmett–Teller (BET) surface areas for TT-COF-1, TT-COF-2, and TT-COF-3 were found to be 501, 2118, and 1107 $m^2 g^{-1}$, respectively. The corresponding pore sizes were initially calculated to be 2.6 nm for TT-COF-1, 2.7 nm for TT-COF-2 and 2.8 nm for TT-COF-3, respectively. PXRD analyses provided further insights into the crystallinity of the COFs. The diffraction patterns for TT-COF-1 (Figure 2a), TT-COF-2 (Figure 2b), and TT-COF-3 (Figure 2c) showed intense and sharp peaks, indicating high crystallinity. Pawley refinement and lattice modeling were employed to optimize the structural parameters, which aligned well with the experimental PXRD profiles. A comparison between observed and simulated PXRD patterns suggested that the TT-COFs had slipped AA stacking (blue), while staggered AB modes did not match the experimental results (Figure S10). The optimized lattice parameters are as follows: TT-COF-1 (a, $b = 29.42157$ Å, $c = 5.51568$ Å, $\alpha = \beta = \gamma = 90°$, $R_{wp} = 7.15\,\%$, $R_p = 5.01\,\%$, space group P6, Figure 2d, Table S2), TT-COF-2 ($a = b = 30.56287$ Å, $c = 3.55287$ Å, $\alpha = \beta = \gamma = 90°$, $R_{wp} = 5.22\,\%$, $R_p = 4.04\,\%$, space group P6, Figure 2e, Table S3), and TT-COF-3

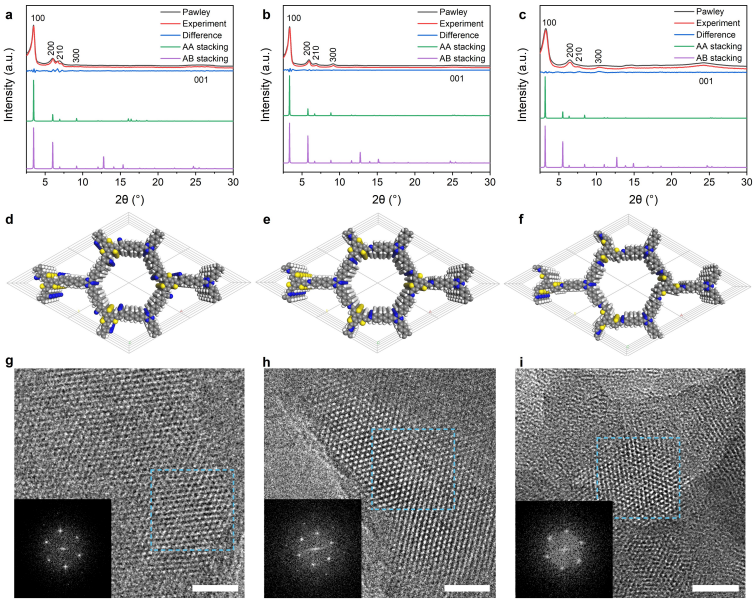

Figure 2. PXRD patterns of (a) TT-COF-1, (b) TT-COF-2, and (c) TT-COF-3. Unit cells of (d) TT-COF-1, (e) TT-COF-2, and (f) TT-COF-3. HR-TEM images of (g) TT-COF-1, (h) TT-COF-2, and (i) TT-COF-3. Scale bars: 20 nm. Insets: the corresponding FFT images.

($a=b=32.06289$ Å, $c=3.53658$ Å, $\alpha=\beta=\gamma=90°$, $R_{wp}=3.86\,\%$, $R_p=2.46\,\%$, space group P6, Figure 2f, Table S4).

High-resolution transmission electron microscopy (HR-TEM) further confirmed the crystalline nature of the pore structures, revealing hexagonal lattice patterns along the [001] direction for all three COFs (Figures 2g–i). These HR-TEM images validate the structural integrity and alignment of the COFs, supporting their potential use in various applications requiring precise structural characteristics.

The electron transfer ability of the TT-COFs was investigated using ultraviolet-visible (UV/Vis) absorption spectroscopy (Figure 3a), which revealed their highly conjugated skeletons. The optical band gaps (E_g) of TT-COF-1, TT-COF-2, and TT-COF-3 were determined to be 2.17, 2.22, and 2.23 eV, respectively (Figure 3b). Mott–Schottky measurements provided the conduction band minimum (CBM) values for TT-COF-1, TT-COF-2, and TT-COF-3, which were found to be −1.15, −1.25, and −1.28 eV, respectively (Figure 3c and 3d). The more negative CBM of TT-COF-3 indicated it had stronger electron reduction capability compared to the other samples.

The thermogravimetric and chemical stability of the TT-COFs were thoroughly assessed to evaluate their performance under various conditions. Thermogravimetric analysis (TGA) demonstrated that the TT-COFs exhibited good thermally stability in a nitrogen atmosphere (Figure S11), which is a critical factor for applications involving high-temperature environments or processes. Additional stability tests involved exposing the TT-COFs to a variety of solutions, including 6 M KOH, 6 M HCl, water, and *N*, *N*-dimethylformamide for 24 hours. These tests were designed to simulate diverse chemical environments, ensuring the robustness of the COFs. Impressively, all three TT-COF maintained their original skeletal structures and crystalline integrity, as confirmed by PXRD patterns, shown in Figure S12, confirming their exceptional chemical stability in harsh conditions.

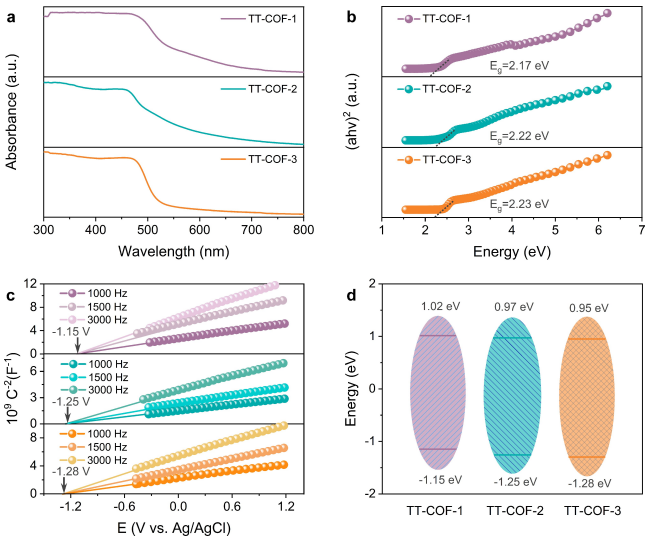

Figure 3. (a) The electron absorption spectra, (b) Tauc plots, (c) Mott–Schottky curves, and (d) schematic energy band structure of TT-COFs.

Furthermore, water contact angle (WCA) measurements for TT-COFs showed that TT-COF-1, TT-COF-2, and TT-COF-3 exhibited WCA values of 66.8°, 60.4°, and 71.8°, respectively (Figure S13). The combination of excellent stability and hydrophilicity provides a strong foundation for their potential applications for electrocatalysis.

To investigate how tunable vertex walls in TT-COFs materials affect ORR performance, the intrinsic catalytic activity and kinetics of the prepared catalysts were evaluated using a rotating disk electrode (RDE) test in an O_2-saturated alkaline electrolyte. The linear sweep voltammetry (LSV) curves recorded at 1600 rpm revealed that TT-COF-3 exhibits a half-wave potential of 0.76 V versus RHE, surpassing both TT-COF-2 (0.72 V) and TT-COF-1 (0.70 V), as shown in Figures 4a, 4h, 4i, and S14. Additionally, the limiting current density of TT-COF-3 ($-3.40\,mA\,cm^{-2}$) significantly exceeded those of TT-COF-1 ($-2.22\,mA\,cm^{-2}$) and TT-COF-2 ($-2.69\,mA\,cm^{-2}$), indicating superior catalytic performance.

The electrochemically active surface areas (ECSAs) were determined through electrochemical double-layer capacitance (C_{dl}) measurements (Figures 4b and S15). Among the samples, TT-COF-3 exhibited the highest C_{dl} value ($5.2\,mF\,cm^{-2}$), which exceeded that of TT-COF-1 ($4.1\,mF\,cm^{-2}$) and TT-COF-2 ($2.1\,mF\,cm^{-2}$). This suggests a greater density of active sites contributing to the catalytic process. Further analysis using Tafel slope measurements based on the LSV curves demonstrated that TT-COF-3 had the lowest Tafel slope ($69\,mV\,dec^{-1}$), indicating it had faster reaction kinetics compared to TT-COF-1 ($88\,mV\,dec^{-1}$) and TT-COF-2 ($113\,mV\,dec^{-1}$) (Figure 4c).

The selectivity of the catalysts was further evaluated through rotating ring-disk electrode (RRDE) measurements. Within the potential range of 0.2–0.8 V, TT-COF-3 achieved a higher electron transfer number ($\sim n=3.8$) compared to TT-COF-1 (~3.0) and TT-COF-2 (~3.4), indicating TT-COF-3 follows a near-complete four-electron reduction process (Figure 4d). Moreover, TT-COF-3 produced a lower H_2O_2 yield (5.0 %) compared to TT-COF-1 (~21 %) and TT-COF-2 (~11 %), further confirming its higher selectivity.

Regarding the kinetic current density (j_k), TT-COF-3 outperformed the others, achieving a j_k of $5.60\,mA\,cm^{-2}$, while TT-COF-1 and TT-COF-2 reached 2.49 and $4.49\,mA\,cm^{-2}$, respectively (Figure 4e), at 0.7 V vs. RHE. The turnover frequency (TOF) at 0.7 V for TT-COF-3 was $0.0056\,s^{-1}$, which was 2.0 and 1.2 times greater than those of TT-COF-1 and TT-COF-2, respectively. The mass activities for TT-COF-1, TT-COF-2, and TT-COF-3 were 8.0, 11.5, and $14.5\,A\,g^{-1}$, respectively, demonstrating that TT-COF-3 exhibits excellent catalytic activity among the tested COFs as well as other reported metal-free COFs (Figure 4f and 4h).[13–17]

Additionally, TT-COF-3 demonstrated excellent methanol resistance, with negligible loss in current density following the addition of methanol for a period of 3000 s (Figure 4g). Over an 18-hour chronoamperometric I-t test, the current density of TT-COF-3 remained at its initial value at 90.8 %, outperforming TT-COF-1 (60.8 %) and TT-COF-

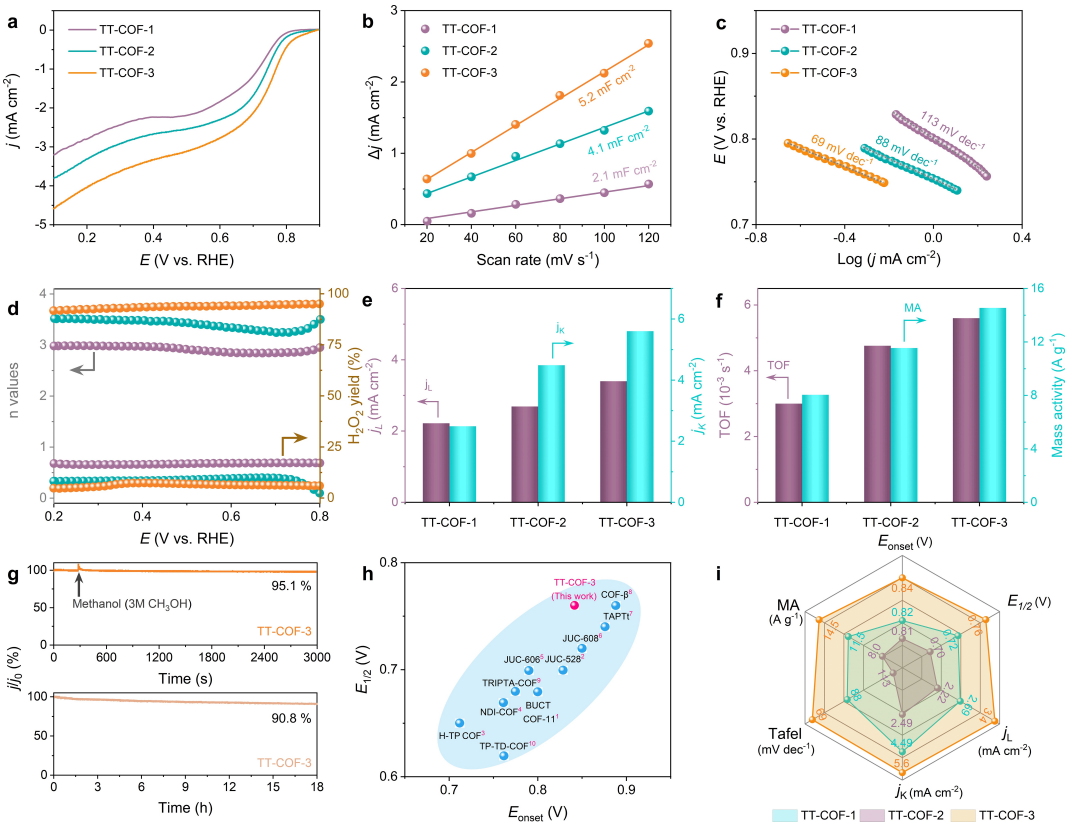

Figure 4. (a) LSV curves, (b) Cdl Values, (c) Tafel slopes, (d) Electron-transfer number and the selectivity, (e) Limiting current density (j_L) and kinetic current density (j_K), (f) TOF values and mass activity, (g) Long-time stability and CH_3OH-poison effect, of TT-COFs. (h) The onset and half-wave potential distributions of previously reported COF catalysts and TT-COF-3. (i) Radar plot showing a comparison of different electrochemical parameters to evaluate the oxygen reduction performance of the three TT-COFs.

2 (85.2 %) (Figures 4g and S16). Overall, TT-COF-3 exhibited superior comprehensive electrochemical performance compared to the other TT-COFs (Figure 4i).

To investigate the catalytic mechanism exhibited by the COFs with tunable vertex walls, density functional theory (DFT) calculations were employed to gain deeper insights into the intrinsic catalytic activities of the potential active sites involved in the ORR process. Gibbs free energy (ΔG) calculations were conducted using VASP software to assess the overpotentials at the seven potential active sites within the three TT-COFs (Figure 5a–e, Tables S5–S7). The thermodynamics and rate-limiting steps of oxygen electrocatalysis catalysed by TT-COFs were elucidated through free energy pathway analysis (Figure 5e). For all three TT-COFs, the rate-determining step in the ORR was identified as the reduction of the *OOH intermediate to form an O_2 molecule (Figures 5d and 5e). During the catalytic ORR process, three intermediate states (*OOH, *O, and *OH) are sequentially formed as oxygen is converted to water (Figure 5d). Notably, four carbon atoms located near and within the pentacyclic thiophene-S units (sites 1 and 4) in the TT-COFs exhibited low ORR overpotentials. This observation highlights the thiophene-S units play role for enhancing the catalytic activity for the ORR.

Specifically, the overpotentials at site 4 in TT-COF-3 were 1.50 eV (Figure 5e), which was lower than those of all sites in TT-COF-1 and TT-COF-2 (Figure 5e and Tables S5–S7). In addition to forming OOH*, TT-COFs require less energy to convert OOH* to OH*. The superior catalytic activity of TT-COF-3 compared to TT-COF-1 and TT-COF-2 is primarily attributed to the modulation of the electronic states of the controllable walls by the introduced pentacyclic thiophene-S units adjacent to carbon, which accelerates the reaction kinetics.

Given the superior ORR performance of TT-COF-3, its practical application as a cathode catalyst was next evaluated in a zinc-air battery (ZAB) in Figure 6a. The TT-COF-3 electrode exhibited an open circuit voltage of 1.3 V (Figure 6b) and demonstrated a maximum power density of 202.5 mW cm^{-2} (Figure 6c), which can be attributed to its favorable mass transfer characteristics—crucial for enhancing the overall performance of ZABs. The specific capacity of the TT-COF-3 electrode was calculated to be 699 mAh g^{-1} (Figure 6d), reinforcing the viability of utilizing COFs as effective catalysts in battery environments.

As the current density increased from 1.0 to 50.0 mA cm^{-2}, the voltage exhibited only a slight decrease, indicating that the ZABs assembled with this material achieved excellent discharge rate performance (Figure 6e). Furthermore, the TT-COF-3 electrode showed stable cycle life, maintaining performance for 600 hours during continuous discharge at a current density of 5.0 mA cm^{-2} (Fig-

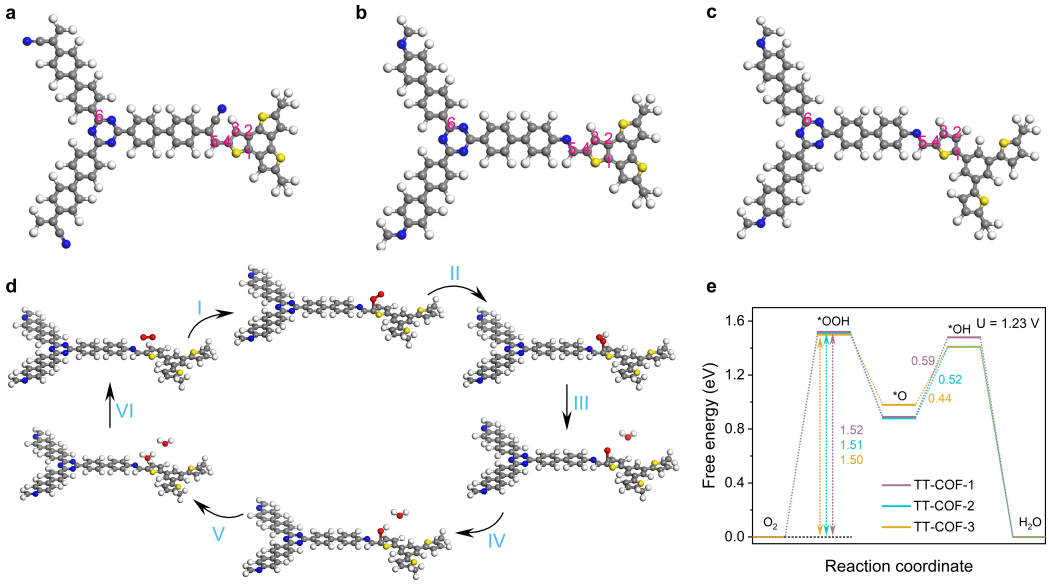

Figure 5. (a–c) Optimized structures of TT-COF-1, TT-COF-2, and TT-COF-3 at the B3LYP/6-31G(d,p) level, (d) Schematic pathway for ORR on TT-COF-3, and (e) Free energy diagrams of ORR for TT-COF-1, TT-COF-2, and TT-COF-3.

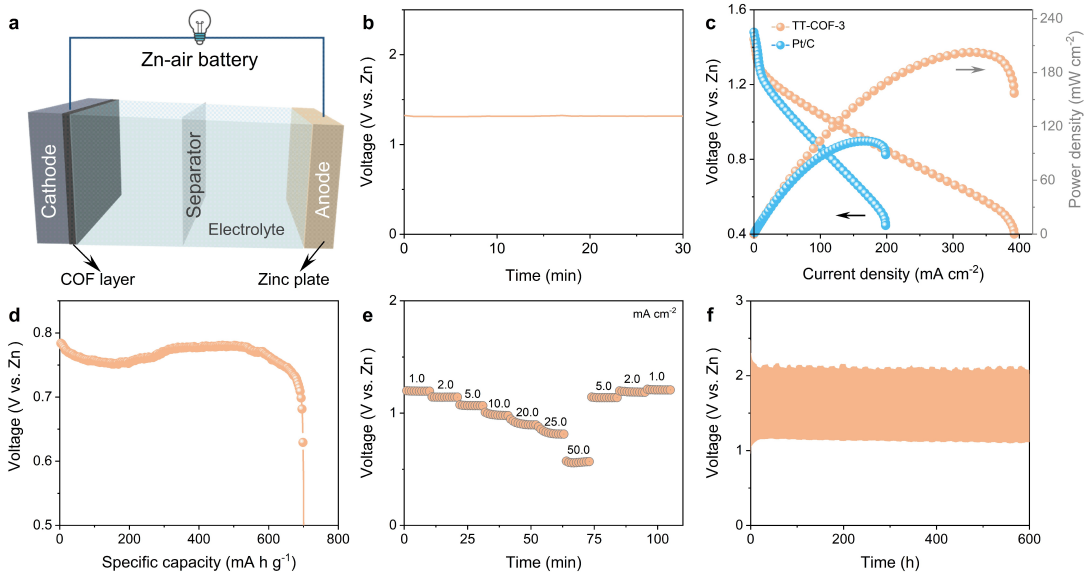

Figure 6. Performance of zinc-air battery assembled with TT-COF-3. (a) Diagram of an aqueous rechargeable ZAB, (b) Open circuit voltage, (c) Power density curves and charge–discharge polarization, (d) Discharge curves at a constant current density of 20 mA cm^{-2}, (e) Rate discharging–charging curves at various current densities, and (f) The durability stability test of the ZAB fabricated with TT-COF-3 measured at 5 mA cm^{-2}.

ure 6f). The impressive stability of TT-COF-3 under continuous discharge conditions suggests its potential as a long-lasting and reliable catalyst for next-generation energy storage technologies.

Conclusions

We demonstrated an approach to tunable catalytic vertex wall chemistry by integrating triazine and thiophene units to enhance COF catalytic performance. This vertex-wall approach allowed the fine-tuning of electronic states, resulting in improved intermediate adsorption properties and accelerated ORR activity. The engineered COF exhibited a half-wave potential of 0.76 V and a mass activity of 14.5 A g^{-1}, outperforming COFs modified by linkers or linkage changes. Theoretical calculations revealed that this enhanced ORR activity is due to the strengthened binding affinity of the OOH* intermediates on the carbon atoms adjacent to the thiophene vertex, facilitating OOH* reduction to O_2 mole-

cules, which is the rate-limiting step of ORR. These findings underscore the advantageous effect of vertex wall regulation, to not only improve ORR performance but also to broaden the design principles for metal-free catalysts in general. By strategically positioning functional groups at structural vertices, we achieved a level of electronic control that opens up new possibilities for designing COFs, and related materials for energy storage applications beyond ORR. This study provides valuable insights into the rational design of COF-based catalysts, positioning them as versatile candidates for next-generation, sustainable energy storage and conversion technologies.

Author Contributions

C. Li, Z. Wang, and Y. Jin contributed equally to this work. C. Li, Y. Jin, and Z. Li performed the primary experiments and data collection. Z. Wang and Z. Lee were responsible for the theoretical calculations. Supporting experiments were conducted by Y. Jin, J.-P. Jeon, S. Zhao, Y. Shao, F. Tang, W.-Y. Kim, R. Guan, and J.-M. Seo. The project was designed by C. Li, Z. Li, S.-Y. Lee, and J.-B. Baek. C. Li, Z. Li, S.-Y. Lee, and J.-B. Baek wrote the manuscript, and all authors discussed the results and provided comments on the manuscript.

Acknowledgements

This work was supported by the research programs (RS-2023-00221668, RS-2024-00435493, RS-2024-00466616) through the National Research Foundation (NRF), and the Institute for Basic Science (IBS-R019-G1) by the Ministry of Science and ICT of Korea.

Conflict of Interest

The authors declare no conflict of interest.

Data Availability Statement

The data that support the findings of this study are available from the corresponding author upon reasonable request.

Keywords: covalent organic framework · oxygen reduction reaction · vertex structure · triazine unit · thiophene unit

[1] a) G. Wu, P. Zelenay, *Acc. Chem. Res.* **2013**, *46*, 1878–1889; b) S. Dey, B. Mondal, S. Chatterjee, A. Rana, S. Amanullah, A. Dey, *Nat. Rev. Chem.* **2017**, *1*, 0098; c) K. Kodama, T. Nagai, A. Kuwaki, R. Jinnouchi, Y. Morimoto, *Nat. Nanotechnol.* **2021**, *16*, 140–147; d) L. Wang, A. Ambrosi, M. Pumera, *Angew. Chem. Int. Ed.* **2013**, *52*, 13818–13821; e) W. Wei, H. Liang, K. Parvez, X. Zhuang, X. Feng, K. Müllen, *Angew. Chem. Int. Ed.* **2014**, *53*, 1570–1574.

[2] a) O. Medina, Z. Wang, R. Cruz-Silva, A. Morelos-Gomez, F. Wang, X. Yao, M. Terrones, M. Endo, *Adv. Mater.* **2019**, *31*, 1805717; b) J. Quílez-Bermejo, E. Morallón, D. Cazorla-Amorós, *Carbon* **2020**, *165*, 434–454.

[3] a) J. Zhang, Z. Zhao, Z. Xia, L. Dai, *Nat. Nanotechnol.* **2015**, *10*, 444–452; b) I.-Y. Jeon, S. Zhang, L. Zhang, H.-J. Choi, J.-M. Seo, Z. Xia, L. Dai, J.-B. Baek, *Adv. Mater.* **2013**, *25*, 6138.

[4] a) C. S. Diercks, O. M. Yaghi, *Science* **2017**, 355, aal1585; b) K. Geng, T. He, R. Liu, S. Dalapati, K. T. Tan, Z. Li, S. Tao, Y. Gong, Q. Jiang, D. Jiang, *Chem. Rev.* **2020**, *120*, 8814–8933; c) H. S. Sasmal, A. Kumar Mahato, P. Majumder, R. Banerjee, *J. Am. Chem. Soc.* **2022**, *144*, 11482–11498; d) H. Gao, A. R. Neale, Q. Zhu, M. Bahri, X. Wang, H. Yang, Y. Xu, R. Clowes, N. D. Browning, M. A. Little, L. J. Hardwick, A. I. Cooper, *J. Am. Chem. Soc.* **2022**, *144*, 9434–9442.

[5] a) J. Li, X. Jing, Q. Li, S. Li, X. Gao, X. Feng, B. Wang, *Chem. Soc. Rev.* **2020**, *49*, 3565–3604; b) F. Haase, B. V. Lotsch, *Chem. Soc. Rev.* **2020**, *49*, 8469–8500; c) Y. Zhu, P. Shao, L. Hu, C. Sun, J. Li, X. Feng, B. Wang, *J. Am. Chem. Soc.* **2021**, *143*, 7897–7902; d) S. Bi, Z. Zhang, F. Meng, D. Wu, J. S. Chen, F. Zhang, *Angew. Chem. Int. Ed.* **2022**, *61*, e202111627; e) C. He, D. H. Si, Y. B. Huang, R. Cao, *Angew. Chem. Int. Ed.* **2022**, *61*, e202207478.

[6] a) T. Zhang, G. Zhang, L. Chen, *Acc. Chem. Res.* **2022**, *55*, 795–808; b) J. Xu, C. Yang, S. Bi, W. Wang, Y. He, D. Wu, Q. Liang, X. Wang, F. Zhang, *Angew. Chem. Int. Ed.* **2020**, *59*, 2384–23853; c) N. Li, D.-H. Si, Q.-j. Wu, Q. Wu, Y.-B. Huang, R. Cao, *CCS Chem.* **2022**, *5*, 1130–1143; d) R. Bao, Z. Xiang, Z. Qiao, Y. Yang, Y. Zhang, D. Cao, S. Wang, *Angew. Chem. Int. Ed.* **2023**, *62*, e202216751; e) H. Su, W. Zhou, W. Zhou, Y. Li, L. Zheng, H. Zhang, M. Liu, X. Zhang, X. Sun, Y. Xu, F. Hu, J. Zhang, T. Hu, Q. Liu, S. Wei, *Nat. Commun.* **2021**, *12*, 6118.

[7] a) M. Guo, X. Guan, Q. Meng, M.-L. Gao, Q. Li, H.-L. Jiang, *Angew. Chem. Int. Ed.* **2024**, *63*, e202410097; b) M. Martínez-Fernández, E. Martínez-Periñán, A. P. Ruigómez, J. J. Cabrera-Trujillo, J. A. R. Navarro, F. A. -Galindo, D. Rodríguez-San-Miguel, M. Ramos, R. Vismara, F. Zamora, E. Lorenzo, J. L. Segura, *Angew. Chem. Int. Ed.* **2023**, *62*, e202313940; c) G. Hu, R. Zhang, Z. Jiang, *Acc. Mater. Res.* **2021**, *2*, 630–643.

[8] a) Q. Zhao, Q. Zhang, Y. Xu, A. Han, H. He, H. Zheng, W. Zhang, H. Lei, U. Apfel, R. Cao, *Angew. Chem. Int. Ed.* **2024**, *63*, e202414104; b) H.-J. Zhu, M. Lu, Y.-R. Wang, S.-J. Yao, M. Zhang, Y.-H. Kan, J. Liu, Y. Chen, S.-L. Li, Y.-Q. Lan, *Nat. Commun.* **2020**, *11*, 497; c) Z. Mei, G. Zhao, C. Xia, S. Cai, Q. Jing, X. Sheng, H. Wang, X. Zou, L. Wang, H. Guo, B. Y. Xia, *Angew. Chem. Int. Ed.* **2023**, *62*, e202303871; d) S. Karak, K. Koner, A. Karmakar, S. Mohata, Y. Nishiyama, N. T. Duong, N. Thomas, T. G. Ajithkumar, M. S. Hossain, S. Bandyopadhyay, S. Kundu, R. Banerjee, *Adv. Mater.* **2024**, *36*, 2209919; e) R. Bao, Z. Xiang, Z. Qiao, Y. Yang, Y. Zhang, D. Cao, S. Wang, *Angew. Chem. Int. Ed.* **2023**, *62*, e202216751; f) J. Tang, C. Su, Z. Shao, *Small Methods* **2021**, *5*, 2100945.

[9] a) M. Borrelli, C. J. Querebillo, D. L. Pastoetter, T. Wang, A. Milani, C. Casari, H. K. Ly, F. He, Y. Hou, C. Neumann, A. Turchanin, H. Sun, I. M. Weidinger, X. Feng, *Angew. Chem. Int. Ed.* **2021**, *60*, 18876–18881; b) X. Li, P. Yadav, K. P. Loh, *Chem. Soc. Rev.* **2020**, *49*, 4835–4866; c) R.-R. Liang, S.-Y. Jiang, R. -Han, X. Zhao, *Chem. Soc. Rev.* **2020**, *49*, 3920–3951.

[10] a) M.-D. Zhang, J.-R. Huang, W. Shi, P.-Q. Liao, X.-M. Chen, *Angew. Chem. Int. Ed.* **2023**, *62*, e202308195; b) D.-G. Wang, T. Qiu, W. Guo, Z. Liang, H. Tabassum, D. Xia, R. Zou, *Energy Environ. Sci.* **2021**, *14*, 688–728; c) X. Zhao, P. Pachfule, S. Li, T. Langenhahn, M. Ye, C. Schlesiger, S. Praetz, J. Schmidt, A. Thomas, *J. Am. Chem. Soc.* **2019**, *141*, 6623–6630; d) X. Wang, X. Ding, Y. Jin, D. Qi, H. Wang, Y. Han, T. Wang, J. Jiang, *Angew. Chem. Int. Ed.* **2023**, *62*, e202302808.

[11] a) K. P. Gong, F. Du, Z. H. Xia, M. Durstock, L. M. Dai, *Science* **2009**, *323*, 760–764; b) D. Guo, R. Shibuya, C. Akiba, S. Saji, T. Kondo, J. Nakamura, *Science* **2016**, *351*, 361–365; c) J.-C. Dong, X.-G. Zhang, V. B. Martos, X. Jin, J. Yang, S. Chen, Z.-L. Yang, D.-Y. Wu, J. Miguel Feliu, C. T. Williams, Z.-Q. Tian, J.-F. Li, *Nat. Energy.* **2019**, *4*, 60–67; d) C.-X. Zhao, X. Liu, J.-N. Liu, J. Wang, X. Wan, C. Wang, X.-Y. Li, Ji. Shui, L. Song, H.-J. Peng, B.-Q. Li, Q. Zhang, *Angew. Chem. Int. Ed.* **2023**, *62*, e202313028.

[12] a) H. F. Wang, L. Chen, H. Pang, S. Kaskel, Q. Xu, *Chem. Soc. Rev.* **2020**, *49*, 1414–1448; b) P. Prabhu, J. M. Lee, *Chem. Soc. Rev.* **2021**, *50*, 6700–6719; c) Wang, J. Chen, Y. Lin, X. Wang, J. Li, Y. Li, L. Gao, L. Zhang, D. Chao, X. Xiao, J. M. Lee, *Adv. Mater.* **2021**, *33*, 2008422; d) H. Wang, J. Li, K. Li, Y. Lin, J. Chen, L. Gao, V. Nicolosi, X. Xiao, J. M. Lee, *Chem. Soc. Rev.* **2021**, *50*, 1354–1390.

[13] a) J. Li, J. Jia, J. Suo, C. Li, Z. Wang, H. Li, V. Valtchev, S. Qiu, X. Liu, Q. Fang, *J. Mater. Chem. A* **2023**, *11*, 18349–18355; b) D. Li, C. Li, L. Zhang, H. Li, L. Zhu, D. Yang, Q. Fang, S. Qiu, X. Yao, *J. Am. Chem. Soc.* **2020**, *142*, 8104–8108; c) X. Yan, B. Wang, J. Ren, X. Long, D. Yang, *Angew. Chem. Int. Ed.* **2022**, *61*, e202209583; d) Z. You, B. Wang, Z. Zhao, Q. Zhang, W. Song, C. Zhang, X. Long, Y. Xia, *Adv. Mater.* **2023**, *35*, 2209129.

[14] a) X. Li, S. Yang, M. Liu, X. Yang, Q. Xu, G. Zeng, Z. Jiang, *Angew. Chem. Int. Ed.* **2023**, *62*, e202304356; b) S. Huang, B. Zhang, D. Wu, Y. Xu, H. Hu, F. Duan, H. Zhu, M. Du, S. Lu, *Appl. Catal. B* **2024**, *340*, 123216.

[15] a) M. Liu, S. Liu, C.-X. Cui, Q. Miao, Y. He, X. Li, Q. Xu, G. Zeng, *Angew. Chem. Int. Ed.* **2022**, *61*, e202213522; b) S. Chang, C. Li, H. Li, L. Zhu, Q. Fang, *Chem. Res. Chin. Univ.* **2022**, *38*, 396–401.

[16] a) J. Li, J. Jia, J. Suo, C. Li, Z. Wang, H. Li, V. Valtchev, S. Qiu, X. Liu, Q. Fang, *J. Mater. Chem. A* **2023**, *11*, 18349–18355; b) X. Yu, Y. Ma, C. Li, X. Guan, Q. Fang, S. Qiu, *Chem. Res. Chin. Univ.* **2022**, *38*, 167–172; c) S. Roy, S. Mari, M. K. Sai, S. C. Sarma, S. Sarkar, S. C. Peter, *Nanoscale.* **2020**, *12*, 22718–22734.

[17] a) S. An, X. Li, S. Shang, T. Xu, S. Yang, C.-X. Cui, C. Peng, H. Liu, Q. Xu, Z. Jiang, J. Hu, *Angew. Chem. Int. Ed.* **2023**, *62*, e202218742; b) Y. J. Yu, Y.-T. Wang, X. Wu, P. Yang, Y. Ma, X.-H. Liu, B. Tang, *Chem. Commun.* **2021**, *57*, 12619–12622; c) S. Royuela, E. M. Periñán, M. P. Arrieta, J. I. Martínez, M. M. Ramos, F. Zamora, E. Lorenzo, J. L. Segura, *Chem. Commun.* **2020**, *56*, 1267–1270; d) F. Liu, H. Li, J. Chen, J. Fei, Z. Yu, Z. Yuan, C. Wang, H. Zheng, Z. Liu, M. Xu, G. Henkelman, L. Wei, Y. Chen, *ACS Nano.* **2021**, *15*, 3309–3319.

Manuscript received: January 6, 2025
Accepted manuscript online: January 21, 2025
Version of record online: ■■, ■■

Research Article

Porous Materials

C. Li, Z. Wang, Y. Jin, Z. Li,* J.-P. Jeon, S. Zhao, Y. Shao, F. Tang, W.-Y. Kim, R. Guan, J.-M. Seo, Z. Lee,* S.-Y. Lee,* J.-B. Baek* **e202500336**

Tunable Catalytic Vertex Wall Chemistry in Metal-free Covalent Organic Frameworks for Enhanced Oxygen Reduction

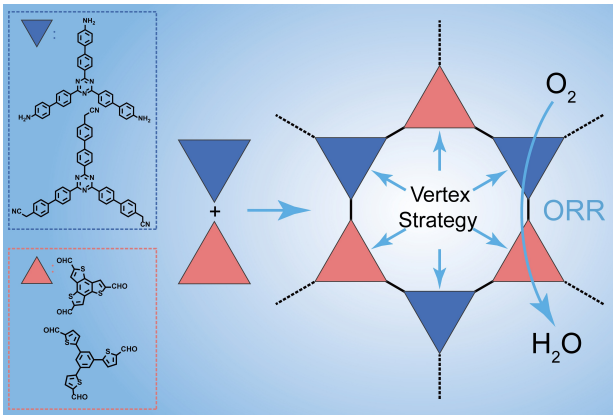

We introduce a tunable catalytic vertex-wall chemistry by incorporating diverse triazine and thiophene units, enabling the precise modulation of COF catalytic performance. This catalytic vertex-wall strategy facilitates the fine-tuning of electronic states, thereby enhancing intermediate adsorption characteristics and accelerating oxygen reduction reaction activity.